Realization of High-Efficiency Inverted Planar Perovskite Solar Cells Based on PEDOT: PSS Doped with Lithium Fluoride

Luqi Chai

School of Physical Engineering, Qufu Normal University, Jining, China.

19558650398@163.com

Abstract. The photovoltaic performance of perovskite solar cells with inverted structure depends on the conductivity of the hole transport layer and the charge transport rate to some extent. To further enhance the effect of the hole transport layer, lithium fluoride (LiF) was doped into poly (3,4-ethylene dioxythiophene)-polystyrene sulfonic acid (PEDOT: PSS) to improve its rate of conductivity and interfacial charge transport. The optimal photoelectric conversion efficiency of LiF-based perovskite solar cells that dope hole transport layer is 20.32% with negligible hysteresis, which is much higher than that of the control group (16.70%). Among all photovoltaic parameters, the improvement of open circuit voltage and fill factor is significant. LiF can not only promote the electrical characteristics of PEDOT: PSS and its hole mobility, but also optimize the quality of the upper perovskite film. Perovskite film shows a crystal orientation more conducive to hole transport on the modified hole transport layer, which obtains a dense and smooth absorption layer film. In this study, PEDOT: PSS-based perovskite solar cells with inverted structure doped with LiF are prepared, which provides a simple and effective method to commercialize perovskite solar cells.

Keywords: Perovskite Solar Cells; Lithium Fluoride; Hole Transport Layer.

1. Introduction

In 2009, Miyasaka first proposed lead halide perovskite ($CH_3NH_3PbI_3$) [1]. Since then, perovskite solar cells have been widely noticed by scientific researchers. So far, the reported highest photoelectric conversion efficiency is 26.0%. Because of its simple structure and excellent performance, perovskite solar cells have emerged in the photovoltaic field, which usually includes formal and inverted structures [2-6]. The electron transport layer composed of titanium oxide and tin oxide, the light absorption layer, and the hole transport layer (HTL) are important components of formal structure [7-9]. Because the bottom of a perovskite solar cell with an inverted structure is a hole transport layer and the top is an electron transport layer, it has many advantages such as simpler preparation conditions, smaller hysteresis, and so on, which enables a broader market prospect [10-14]. In recent years, scientists have researched a lot on the performance of perovskite solar cells with inverted structures, but their efficiency still lags behind that of traditional perovskite solar cells with formal structures. This is mainly due to the physical and chemical properties of hole transport materials in perovskite solar cells with inverted structures, especially the surface properties, such as roughness, which affect the initial nucleation and later crystal growth of perovskite layers; Secondly, the key factor limiting its performance improvement is the large opening voltage loss caused by non-radiation recombination; Finally, the hole transport layer still has the low charge mobility [15-17].

In recent years, researchers have conducted abundant in-depth research on improving the performance of perovskite solar cells with inverted structures by material modification and promoting the preparation process. Sun et al. modified hole transport materials such as poly (3,4-ethylene dioxythiophene)-polystyrene sulfonic acid (PEDOT:PSS) by introducing rubidium chloride (RbCl). RbCl can induce the phase separation of PEDOT:PSS, thus boosting the conductivity of the hole transport layer [18]. In addition, with similar polyhedral structure and lattice parameters to perovskite, RbCl is beneficial to the nucleation and grain growth of perovskite. However, due to the narrow band gap and low transmittance of the inorganic hole transport layer, its conductivity and device efficiency are difficult to be further improved. According to many reports of modified hole transport materials, PEDOT:PSS has been widely used in organic-inorganic hybrid perovskite solar cells because of its excellent optical transparency, good stability, high conductivity, and suitable level position. However,

the insulation properties of PSS seriously undercut the conductivity of PEDOT:PSS. The properties of PEDOT and its influence on the growth of perovskite grains can not be ignored. Jiang et al. reported that the combination of PEDOT:PSS and cesium iodide significantly improved hole extraction and inhibited surface recombination, thus reducing non-radiative recombination loss. However, these methods fail to effectively improve the low conductivity and surface morphology of PEDOT:PSS [19]. Therefore, it is necessary to design a simple method to enhance the hole transport materials, such as using additives to improve the growth platform of perovskite and promote the charge mobility of the hole transport layer.

In this study, we provide an effective method to improve the photoelectric conversion efficiency of perovskite solar cells with inverted structure by adding LiF with positive and negative electrical properties into the precursor solution of hole transport materials. Besides, the filling factor (FF) and voltage of the open circuit (VOC) are obviously promoted. Unexpectedly, LiF not only improves the electrical properties of PEDOT:PSS through phase separation, but also changes the nucleation and growth of perovskite materials on the hole transport layer, which significantly increases the hole transport capacity at the interface. The optimal efficiency of PEDOT:PSS-based devices increased from 16.70% to 20.32%, and VOC and FF also surprisingly increased to 1.14 V and 76.54%.

2. Experimental Section

2.1 Preparation of Materials

Substrate doped with Indium Tin Oxide (ITO), lead iodide (PbI_2), lead bromide ($PbBr_2$), methyl ammonium chloride (MACl), methyl ammonium bromide (MABr), formamidine iodine (FAI), cesium iodide (CsI), dimethyl formamide (DMF), and dimethyl sulfoxide (DMSO) were all purchased from Yingkou Selected New Energy Technology Co., Ltd.; LiF was purchased from Sinopharm Chemical Reagent Co., Ltd.; SnO2 colloidal solution with 15% mass fraction was purchased from Alfa Aesar (China) Chemical Co., Ltd.; [6, 6]-phenyl-C61-PC61BM and poly (3,4-ethylene dioxythiophene)-PEDOT:PSS were purchased from p-OLED Co., Ltd. PbI2 (0.429 g), PbBr2 (0.0265 g), MACl (0.02 g), MABr (0.0074 g), FAI (0.2173 g), and CsI (0.0182 g) were mixed in 1 mL mixed solvent of DMSO:DMF (2:8) for 3 hours to prepare the solution of perovskite film precursor.

2.2 Device Fabrication

ITO conductive glass substrate was cleaned by ultrasonic with a special cleaning solution, acetone, and absolute ethanol in the ultrasonic container for 20 minutes each. Then, it was treated with ultraviolet ozone for 20 minutes to remove the organic residue on the surface. After that, PEDOT:PSS solution with and without LiF was rotated on clean ITO conductive glass at a speed of 5000 rpm for 40 seconds, and annealed in air at 120 °C for 15 minutes. The perovskite precursor solution (80 μL) was then spin-coated step by step for 10 seconds at 1000 rpm and 30 seconds at 5000 rpm. Besides, 150 μL chlorobenzene was dripped onto the substrate 15 seconds before the end of the procedure. Then, it was annealed at 100 ℃ for an hour. After cooling to room temperature, 45 μL PCBM solution was extracted, which was dissolved in chlorobenzene at a concentration of 20 mg/ml. Then, it was spin-coated on perovskite film at a speed of 3000 rpm for 30 seconds. Finally, a 150 nm silver electrode was thermally evaporated on the top of the device.

2.3 Characterization

The current-voltage characteristic (J-V) curves of the device were measured at 100 mW cm-2 using AM 1.5G light source. The external quantum efficiency (EQE) measurement system (QEX10, PV measurement) was used to measure the spectral response of solar cells. SEM images were obtained by FEI Noval-200 scanning electron microscope (SEM). The X-ray diffraction (XRD) was measured by the Shimadzu XRD-7000 diffractometer. The ultraviolet-visible (UV) absorption spectra were measured by the Shimadzu UV-2450 absorption spectrophotometer. Oxford Instruments (MFP-3D-

BIO) were used to measure Atomic Force Microscope (AFM). The photoluminescence spectra were analyzed under the excitation of a 488 nm CW laser. X-ray photoelectron spectroscopy (XPS) was measured on an ESCALAB 250 Xi device.

3. Results and Discussions

The device structure in this experiment is shown in Figure l(a) that ITO/PEDOT:PSS (LiF)/CsFAMA/PCBM/Ag. Different concentrations of LiF are added to PEDOT:PSS and labeled as LiF-x, where x represents the concentration of the solution formed by different amounts of LiF added. As shown in Table 1, the cells prepared under different lithium fluoride doping amounts were analyzed and their optimal photovoltaic performance was analyzed. With the increasing LiF doping amount, the photovoltaic performance of the device changes. With the LiF doping amount increasing to 3 mg ml-1, the optimal photoelectric conversion efficiency increased from 16.70% to 20.32%. The improvement of FF and VOC achieves higher PV conversion efficiency, but excessive doping concentration will lead to a slight decline in PV performance. In other words, when the doping concentration is 5 mg ml-1, the average PV conversion efficiency is only 18.13%. Figure 1(b) is the J-V characteristic curve of a perovskite solar cell prepared based on PEDOT:PSS and optimized LiF-PEDOT:PSS. Under the optimal conditions, the optimal photoelectric conversion efficiency, VOC, FF, and short circuit current density (JSC) of the control group are 16.70%, 1.07 V, 69.29%, and 22.60 mA cm-2 respectively. The highest photoelectric conversion efficiency of the device based on LiF-doped hole transport materials, JSC, VOC, and FF is 20.32%, 23.15 mA cm-2, 1.14 V, and 76.54% respectively. The external quantum efficiency (EQE) spectrum in Figure 1(c) shows that two types of perovskite solar cells have higher photoelectric conversion efficiency in the range of 350-800 nm. Meanwhile, the perovskite solar cells based on LiF-PEDOT:PSS have a higher response than the control cells. The JSC values of the perovskite solar cell based on LiF-PEDOT:PSS and the control cell calculated by EQE are 23.88 and 23.49 mA cm-2 respectively, which are close to the data obtained by the J-V curve. At the same time, according to Figure 1(d), the photoelectric conversion efficiency of perovskite solar cells based on LiF-PEDOT:PSS is 19.72% under reverse scanning and 20.32% under forward scanning. This shows that hysteresis is effectively suppressed compared with control devices [20, 21].

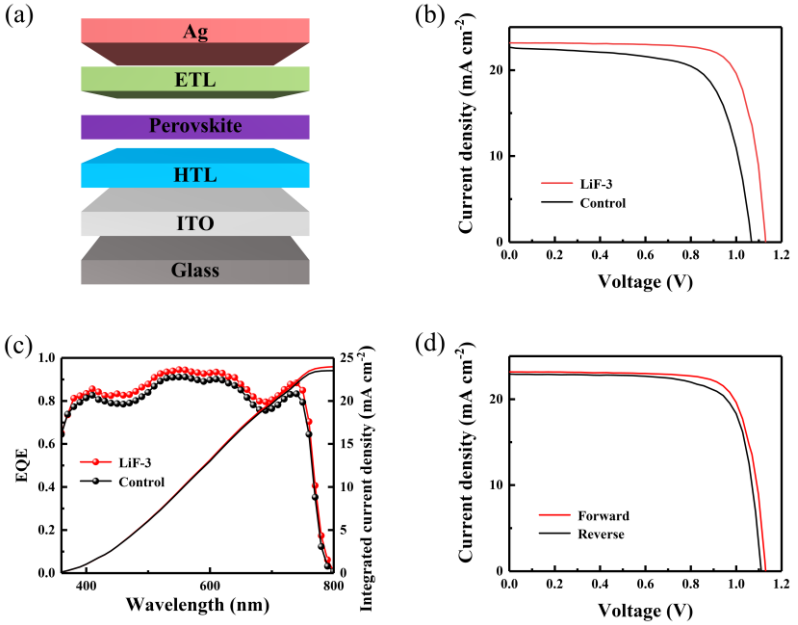

Figure 1 (a) Structure of Inverted Perovskite Solar Cell Device; (b) J-V Curves of Perovskite Solar Cells Based on PEDOT: PSS and LiF-3 PEDOT: PSS; (c) EQE Curves of Perovskite Solar Cells Based on PEDOT: PSS and LiF-3 PEDOT: PSS and Their Integrated Currents; (d) J-V Curves of Forward and Reverse Scanning of LiF-3 PEDOT: PSS Perovskite Solar Cells.

Table 1 Photovoltaic Performance of Perovskite Solar Cells Prepared by LiF-PEDOT: PSS Thin Films with Different Concentrations (mg mL^{-1})

PSCs	V_{OC} (V)	J_{SC}(mA cm^{-2})	FF (%)	PCE (%)
Control	1.07	22.60	69.29	16.70
LiF-1	1.09	22.98	71.61	17.86
LiF-3	1.14	23.15	76.54	20.32
LiF-5	1.10	22.61	73.20	18.13

To further explore the influence trend of surface topography on performance, AFM images of PEDOT:PSS and LiF-3 PEDOT:PSS are shown in Figure 2(a) and Figure 2(b). It can be seen that the roughness of the two films is 6.27 nm and 4.91 nm respectively. Due to the introduction of LiF, the surface roughness decreases slightly. As shown in Figure 2(c), compared with the original PEDOT:PSS, the LiF-PEDOT:PSS sample obtained an obvious signal of 685.7 eV, belonging to element F, which indicates that LiF was doped into [22, 23] as expected.

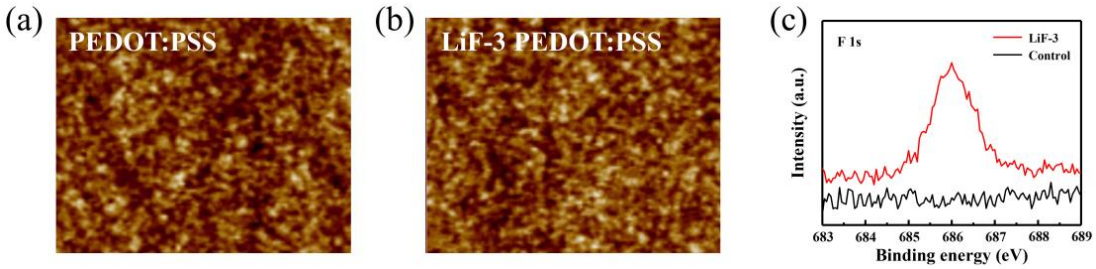

Figure 2 AFM Images Based on (a) PEDOT: PSS and (b) LiF-3 PEDOT: PSS Films; (c) XPS Spectra of F 1s in PEDOT: PSS Films.

The transmission spectra of PEDOT:PSS films with different doping amounts of LiF are shown in Figure 3(a). It can be seen that the influence of LiF on the optical properties of PEDOT:PSS thin films can be neglected. In the visible light range, both the control film and LiF-3 PEDOT:PSS film showed higher transmittance. LiF-3 PEDOT:PSS thin film has excellent optical transmittance, so the optical loss on the front side of the perovskite solar cell with an inverted structure is very small, which helps more photons to be absorbed by the perovskite layer. However, when excessive LiF is introduced, the transmittance decreases. Besides, when the maximum doping concentration is 5 mg ml-1, the optical transmittance is the lowest [24]. To investigate the reason for the decreasing transmittance of PEDOT:PSS film, the corresponding band gap (Eg) of the film can be calculated according to the parameters and equations.

$$(\alpha h\nu)^2=h\nu-E_g \quad (1)$$

Where α is the absorption coefficient, Eg is the difference between the bottom of the conduction band and the top of the valence band, h is the Planck constant, and v is frequency. Figure 3(b) shows the changes of $(\alpha h\nu)^2$ and hν in PEDOT: PSS thin films. The optical band gaps of PEDOT:PSS and LiF-3 PEDOT:PSS are 2.05 and 2.08 eV respectively.

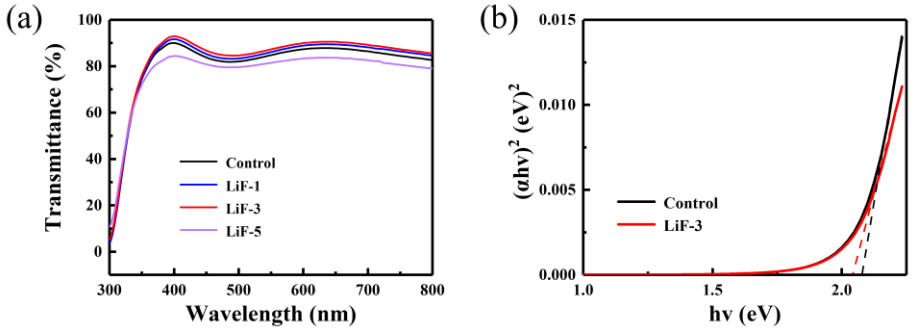

Figure 3 (a) Transmission Spectra of PEDOT: PSS Thin Films with Different LiF Doping Concentrations; (b) The Band Gap Diagrams of PEDOT: PSS and LiF-3 PEDOT: PSS Films.

Then the surface morphology of perovskite thin films deposited on two kinds of hole transport layers was studied by SEM, as shown in Figure 4(a) and Figure 4(b). It can be observed that the surfaces of the two-hole transport layers are completely covered by perovskite layers. In addition, according to AFM images, due to the phase separation of PEDOT and PSS by LiF, the order and crystallinity of PEDOT in the nano-size region are increased, which provides a good growth platform for perovskite crystals. After introducing LiF, the average grain size of perovskite increases. The increasing grain boundaries mainly result from the existence of small grains. Besides, the existence of grain boundaries greatly increases the non-radiative recombination of the whole device, thus reducing various photovoltaic parameters [25, 26]. The introduction of LiF in PEDOT:PSS can inhibit the recombination of carriers.

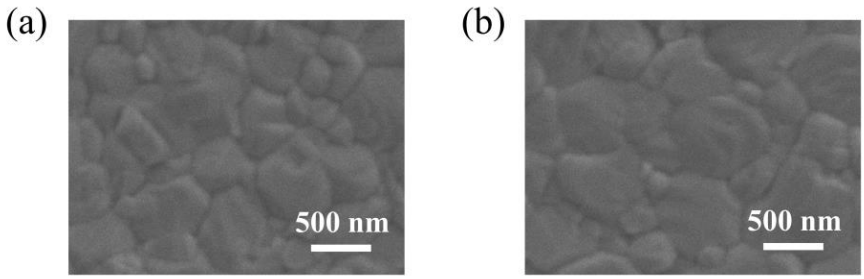

Figure 4 Perovskite Films deposited on (a) PEDOT: PSS and (b) LiF-3 PEDOT: PSS.

The ability to separate and transport electrons and holes is the key factor that determines the performance of perovskite solar cells. The J-V curve of the device with ITO/HTL/Ag structure is shown in Figure 5a. It can be seen that the device based on LiF-PEDOT:PSS has a higher current density, which proves its better hole transmission performance. XPS tests also show that the conductivity of the device based on LiF-PEDOT:PSS is improved compared to the control group. Figure 5(b) shows the XPS signal of S 2p of PEDOT and PSS, the peak at ~ 168 eV belongs to the sulfur atom of PSS, and the peak at 162 ~ 165 eV belongs to the sulfur atom of PEDOT. After adding LiF, the S peaks of the PEDOT chain and PSS chain move in the direction of smaller binding energy. This redshift indicates that the change in the chemical environment around the S atom in PEDOT:PSS is related to the phase separation between PEDOT and PSS. In addition, LiF doping caused the shift of the S 2p peak, but the redshift of S 2p was larger in PSS. It is shown that the PSS chain has been affected by the introduction of dopants, which reduces the negative charge of the PSS chain. This indicates that PSS is not removed after phase separation caused by LiF doping, but maintains and adjusts its interaction with PEDOT chain and morphology. It is also shown that when LiF is doped, PEDOT is no longer completely in the previous insulated environment, but most of it gets rid of the bondage of insulated PSS. Therefore, the charge can be effectively transported between PEDOT, thus improving the carrier mobility and hole collection ability of HTL [30].

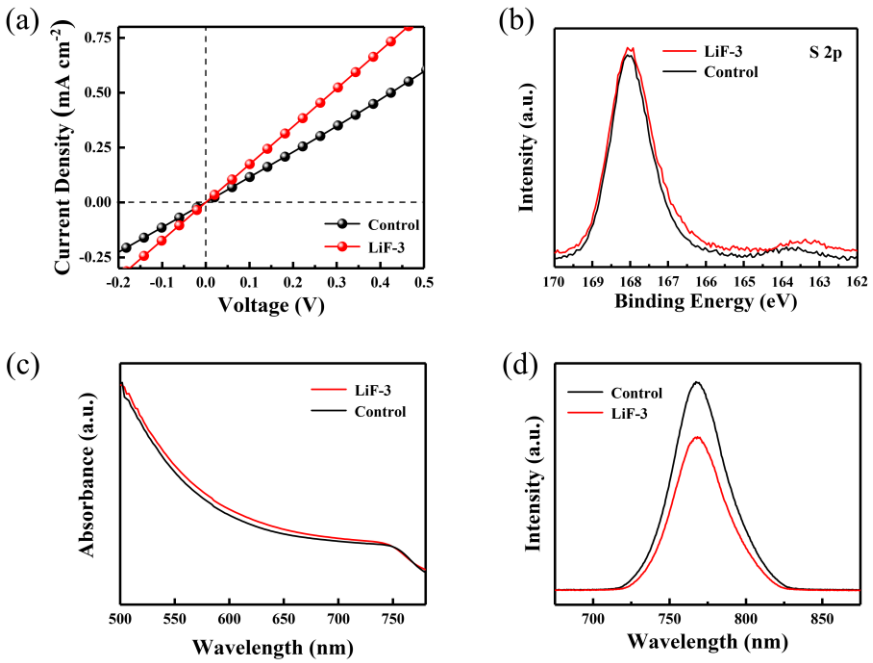

Figure 5 (a) J-V Curves of ITO/HTL/Ag Structural Devices; (b) XPS Spectra of PEDOT: PSS and LiF-3 PEDOT: PSS Films S 2p; (c) Optical Absorption Spectra and (d) Steady PL Spectra of Perovskite Films Prepared on PEDOT: PSS and LiF-3 PEDOT: PSS.

The absorption spectra of devices based on ITO/HTL/CsFAMA structure are shown in Figure 5(c), which lays a foundation for understanding the improvement of charge transfer by introducing LiF into PEDOT:PSS. The absorption intensity of perovskite films deposited on LiF-PEDOT:PSS increased slightly, indicating that the introduction of LiF optimized the crystal orientation of the upper perovskite films, which was consistent with SEM results. Figure 5(d) shows the luminescence spectra of PEDOT: PSS/CsFAMA and LiF-PEDOT: PSS/CsFAMA. The PL intensity of LiF-PEDOT: PSS/ CsFAMA is improved, which indicates that the introduction of LiF into PEDOT: PSS enhances the separation and transfer of charge in perovskite solar cells [31].

To sum up, LiF-doped PEDOT:PSS is beneficial to the formation of CsFAMA and optimizes the crystal orientation, which makes the size distribution of perovskite grain more uniform. In addition, the hole extraction and transport performance of LiF-modified PEDOT:PSS are enhanced.

4. Summary

In this study, it is found that the perovskite solar cells with inverted structure can be obtained by adding a proper amount of LiF into PEDOT: PSS based on the positive and negative ion properties of LiF. In addition, LiF can also make CsFAMA form a new crystal orientation in PEDOT:PSS, thus enhancing the charge extraction and transport at the interface. This research provides a new strategy for the preparation of high-performance HTL to optimize the perovskite absorption layer and improve the charge transport, which is beneficial to commercialize perovskite solar cells as soon as possible.

References

[1] Kojima A, Teshima K, Shirai Y, et al. Organometal halide perovskites as visible-light sensitizers for photovoltaic cells. Journal of the American Chemical Society. Vol. 131 (2009) p. 6050-6051.

[2] Ma F, Zhao Y, Li J, et al. Nickel oxide for inverted structure perovskite solar cells. Journal of Energy Chemistry. Vol. 52 (2021) p. 393-411.

[3] Zhang Y, Li C, Bi E, et al. Efficient inverted perovskite solar cells with a low-dimensional halide/perovskite heterostructure. Advanced Materials Research. Vol. 12 (2022) p. 2202191.

[4] Huang Y, Yan K, Niu B, et al. Finite perovskite hierarchical structures via ligand confinement leading to efficient inverted perovskite solar cells. Energy & Environmental Science. Vol. 16 (2023) p. 557-564.

[5] Kang Y, Na S, et al. Multi-site passivation-based antisolvent additive engineering with gradient distribution for superior triple cation P-I-N perovskite solar cells. Nano Energy. Vol. 97 (2022) p. 107193.

[6] Cheng H, Liu C, Zhuang J, et al. KBF4 additive for alleviating microstrain, improving crystallinity, and passivating defects in inverted perovskite solar cells. Advanced Functional Materials. Vol. 32 (2022) p. 2204880.

[7] Xiong L, Guo Y, Wen J, et al. Review on the application of SnO2 in perovskite solar cells. Advanced Functional Materials. Vol. 28 (2018) p. 1802757.

[8] Chen Y, Zuo X, He Y, et al. Dual passivation of perovskite and SnO2 for high-efficiency MAPbI3 perovskite solar cells. Advanced Science. Vol. 8 (2021) p. 2001466.

[9] Shen D, Pang A, Li Y, et al. Metaltorganic frameworks at interfaces of hybrids perovskite solar cells towards enhanced photovoltaic properties. Chemical Communications. Vol. 54 (2013) p. 1253-1256.

[10] Zhang M, Chen Q, Xue R, et al. Reconfiguration of interfacial energy band structure for high-performance inverted structure perovskite solar cells. Nature Communications. Vol 10 (2019) p. 1-9.

[11] Liu S, Biju V P, Qi Y, et al. Recent progress in the development of high-efficiency inverted perovskite solar cells. NPG Asia Materials. Vol. 15 (2023) p. 27.

[12] Xu J, Dai J, Dong H, et al. Surface-tension release in PTAA-based inverted perovskite solar cells. Organic Electronics. Vol. 100 (2022) p. 106378.

[13] Dou J, Song Q, Ma Y, et al. Improved interfacial adhesion for stable flexible inverted perovskite solar cells. Journal of Energy Chemistry. Vol. 76 (2023) p. 288-294.

[14] Marand R Z, Kermanpur A, Karimzadeh F, et al. Structural and electrical investigation of cobalt-doped NiOx/perovskite interface for efficient inverted solar cells. Nanomaterials. Vol. (2020) p. 872.

[15] Wali Q, Iftikhar J F, Khan E M, et al. High efficiency (>20%) and stable inverted perovskite solar cells: current progress and future challenges. Journal of Materials Chemistry C. Vol. 10 (2022) p. 12908-12928.

[16] Mehdi H, Matheron M, Mhamdi A, et al. Effect of the hole transporting layers on the inverted perovskite solar cells. Journal of Materials Science-Materials in Electronics. Vol. 32 (2021) p. 21579-21589.

[17] Li X, Zhang W, Guo X, et al. Constructing heterojunctions by surface sulfidation for efficient inverted perovskite solar cells. Science. Vol. 375 (2022) p. 434-437.

[18] Liu X, Li B, Zhang N, et al. Multifunctional RbCl dopants for efficient inverted planar perovskite solar cell with ultra-high fill factor, negligible hysteresis and improved stability. Nano Energy. Vol. 53 (2018) p. 567-578.

[19] Jiang K, Wu F, Zhang G, et al. Inverted planar perovskite solar cells based on CsI-dope PEDOT:PSS with efficiency beyond 20% and small energy loss. Journal of Materials Chemistry A. Vol. 7 (2019) p. 21662-21667.

[20] Qi Y, Ndaleh D, Meador E W, et al. Interface passivation of inverted perovskite solar cells by dye molecules. ACS Applied Energy Materials. Vol. 4 (2021) p. 9525-9533.

[21] Zhu Y, Wang S, Ma R, et al. The improvement of inverted perovskite solar cells by the introduction of CTAB into PEDOT:PSS. Solar Energy. Vol. 188 (2019) p. 28-34.

[22] Liu Y, Wang J, Wang F, et al. Full-frame and high-contrast smart windows from halide-exchanged perovskites. Nature Communications. Vol. (2021) p. 3360.

[23] Du R, Wang J, Wang Y, et al. Unveiling reductant chemistry in fabricating noble metal aerogels for superior oxygen evolution and ethanol oxidation. Nature Communications. Vol. 11 (2020) p. 1590.

[24] Jiao L, Howard S, Ran S, et al. Chiral superconductivity in heavy-fermion metal UTe2. Nature. Vol. 579 (2020) p. 523-527.

[25] Chen H, Zhu L, Xue C, et al. Efficient and bright warm-white electroluminescence from lead-free metal halides. Nature Communications. Vol. 12 (2021) p. 1421.

[26] Shao Z, Li Y, Liu C, et al. Reversible interconversion between methanol-diamine and diamide for hydrogen storage based on manganese catalyzed (de)hydrogenation. Nature Communications. Vol. 11 (2020) p. 591.

[27] Wang J, Luo S, Lin Y, et al. Templated growth of oriented layered hybrid perovskites on 3D-like perovskites. Nature Communications. Vol. 11 (2020) p. 582.

[28] Ye Y, Yin Y, Chen Y, et al. Metal-organic framework materials in perovskite solar cells: recent advancements and perspectives. Small. (2023) p. 2208119.

[29] Xing P, Niu Y, Mu R, et al. A pocket-escaping design to prevent the common interference with near-infrared fluorescent probes in vivo. Nature Communications. Vol. 11 (2020) p. 1573.

[30] Wang L, Zhou H, Hu J, et al. A Eu3+-Eu2+ ion redox shuttle imparts operational durability to Pb-I perovskite solar cells. Science. Vol. 363 (2019) p. 265-270.

[31] Wang F, Chang Q, Yun Y, et al. Hole-transporting low-dimensional perovskite for enhancing photovoltaic performance. Research. Vol. 2021 (2021) p. 9797053.